2007 IEEE International Conference on
Robotics and Automation
Roma, Italy, 10-14 April 2007

Needle Insertion Point and Orientation Optimization in Non-linear Tissue with Application to Brachytherapy

Ehsan Dehghan and Septimiu E. Salcudean

Abstract— **This paper presents a new method of optimizing the needle insertion point, heading and depth for needle insertion into deformable tissue. The goal is to minimize the distance between a number of specified targets and the needle. Assuming a rigid needle and a deformable tissue described by a finite element model, an iterative optimization method is proposed that uses the needle insertion simulation. At each iteration, the best fitted 3D line to the targets in the simulated deformed configuration is used as a candidate for the new insertion line in the next iteration. This method has been implemented in a prostate brachytherapy simulator to minimize seed misplacement errors. The targets are designed to lie on a straight line in the undeformed configuration inside the prostate. To increase the accuracy while simulating the prostate rotation, a non-linear model is used. The neo-Hookean material model is exploited to determine the effects of geometric and mechanical non-linearities and compressibility effects. It is shown that the optimization algorithm converges in few iterations and decreases the targeting error effectively.**

I. INTRODUCTION

Prostate cancer is the most common cancer in men. Low dose brachytherapy is an effective treatment for localized prostate cancer. During brachytherapy, radioactive capsules or "seeds" of ^{125}I or ^{103}Pd are permanently placed inside the prostate and peri-prostatic tissue, with the goal of delivering sufficient radiation to kill the cancerous tissue while maintaining a tolerable dose to the urethra and rectum. In a common approach, the seed positions inside the tissue are planned before the operation. First, during a volume study, images of the prostate are taken using trans-rectal ultrasound (TRUS). A 3D model of the prostate tissue is constructed using several parallel TRUS images that are manually segmented. This model is then used for treatment planning. The seed positions are usually along straight lines parallel to the long axis (y axis) of the TRUS probe (see Fig. 1). The physician implants the seeds using long needles inserted according to the plan with the aid of a guiding template. The template has holes in the $x-z$ plane, allowing the needles to move along the y axis. Real time TRUS imaging and X-ray fluoroscopy are used by physicians to guide the needle during the operation.

During brachytherapy, needle insertion forces deform the prostate tissue and displace the targeted seed positions. Due to needle forces the prostate can rotate up to 20 degrees [1]. As a result of prostate movement, seed misplacement errors are still common in brachytherapy [2], leading to underdosed regions and complications, such as impotence or urinary incontinence. Limited visual feedback during the operation demands highly skilled physicians to compensate for the deformations and decrease the errors. Hence, brachytherapy simulators and planners are in demand to train physicians and provide treatment plans. In addition, brachytherapy planners can be used for robotic needle insertion.

The guiding template allows the needle to move along the y axis. Although the target positions are originally along the lines parallel to this axis, they diverge from this line due to tissue deformation. Therefore, insertion of the needle at a different orientation can decrease the error between the predefined target positions and the actual seed locations. Upon availability of a robotic system [3] to place and orient the needle, the needle orientation and insertion point can be optimized to maximize the targeting accuracy in the presence of tissue deformation.

The focus of this paper is on the optimization of the needle insertion point, heading and depth for insertion of a rigid needle into a 3D prostate model to minimize the seed misplacement errors. Although the brachytherapy needle is slightly flexible, this insertion point and heading can be used as a starting point for needle planning algorithms that account for needle flexibility. This optimization method is based on simulation. The Finite Element Method (FEM) is used for the needle insertion simulation. A non-linear model that considers geometric and mechanical non-linearities is used in the FEM simulations.

This paper is organized as follows. In the next section, previous work on needle insertion simulation and planning is presented. The needle insertion simulation method and the non-linear model used are introduced in the third section. The fourth section is dedicated to the optimization approach, followed by the simulation results and conclusions.

II. RELATED WORK

The Finite Element Method is known to be a very powerful tool to simulate tissue deformations during surgery and needle insertion. This method has been used in 2D and 3D needle-tissue interaction simulations [4]–[6]. A 3D mesh of prostate tissue was generated in [5] and then used to simulate the brachytherapy procedure using a linear FEM model and accelerated simulation methods. Alterovitz *et al.* used a 2D linear FEM model to simulate needle insertion during brachytherapy [6]. They also used a search-based sensorless

This work was supported by the National Sciences and Engineering Research Council of Canada and by a PRECARN scholarship.

E. Dehghan is with the Department of Electrical and Computer Engineering, University of British Columbia, Vancouver, BC, Canada ehsand@ece.ubc.ca

S.E. Salcudean is with Faculty of Electrical and Computer Engineering, University of British Columbia, Vancouver, BC, Canada tims@ece.ubc.ca

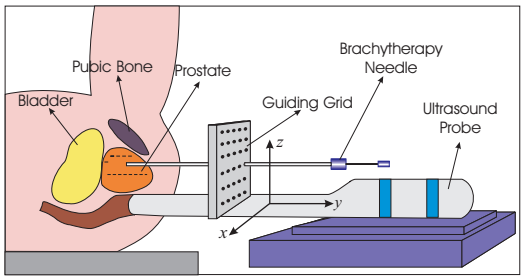

Fig. 1. Insertion of the needle during prostate brachytherapy

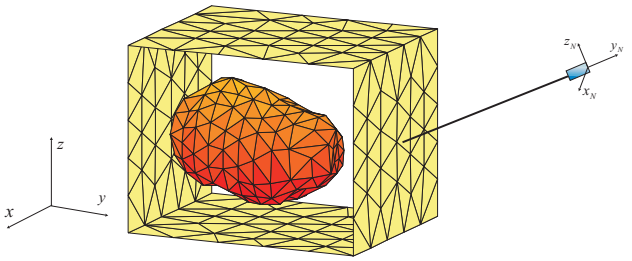

Fig. 2. The simplified mesh of prostate and surrounding tissue.

planning algorithm to optimize the needle insertion point to minimize the seed placement error in a 2D brachytherapy simulator [7]. Unlike in the approach presented here, their method did not optimize the needle insertion angle.

The same group also worked on optimizing the needle insertion initial location and orientation for a highly flexible bevel-tip needle model introduced by Webster *et al.* [8] in 2D tissue using a penalty method [9]. To solve the unconstrained optimization problem generated by the penalty method they used the Gradient Descent algorithm. Due to its complexity, the objective function cannot be differentiated directly. To approximate the derivatives of the objective function with respect to the optimization parameters at each point, they simulated the needle insertion procedure with perturbed parameters. By contrast, the algorithm proposed in this paper is gradient free and converges in few iterations.

Alterovitz *et al.* also used the needle bevel tip direction as an input and guided a highly flexible needle inside a 2D tissue model under Markov uncertainty [10] without the optimization of the initial location or orientation. The highly flexible model, that assumes that the needle is steered by its tip without generating significant lateral forces on the tissue, is not applicable to brachytherapy or many other needles used in practice.

DiMaio and Salcudean, introduced the concept of steering a flexible needle inside tissue by manipulating its base [11]. They guided a flexible needle inside a 2D tissue phantom to reach a target while avoiding obstacles using a numerically computed needle Jacobian and potential fields. Glozman and Shoham [12] used a 2D spring mesh to simulate the tissue and a linear beam to simulate the needle flexibility. They derived the inverse kinematics of the needle to steer the needle inside the tissue. However, in [11] and [12] the initial needle location and orientation were not optimized. The optimization method introduced in this paper can define the initial needle placement for the above mentioned flexible needle steering methods.

A comparison of different models for brachytherapy needles was presented in [13]. In [14] and [15] needle rotation, speed and acceleration were controlled to reduce the tissue deformation during insertion. Heverly *et al.* [15] used an energy based fracture mechanics approach to show that the velocity dependence of tissue properties can reduce tissue motion with increased needle velocity.

Okamura *et al.* [16] divided the force applied by the tissue to the needle into three parts: 1) capsule stiffness; 2) friction and 3) cutting forces occurring at the needle tip. The tip and friction forces applied by a needle during penetration into a canine prostate were measured by Kataoka *et al.* [17]. DiMaio and Salcudean measured the force profile along the needle during penetration into a slab of PVC [4]. They used this profile to introduce a stick-slip interaction model between needle and tissue [4]. This needle-tissue interaction model is used in this paper.

Linear FEM models are not rotation invariant and cannot accurately simulate situations with large rotations and high strains. However, large rotations and high strains can occur during brachytherapy [1]. To achieve higher accuracies in this case, geometric and mechanical non-linearities should be taken into account. Geometric and mechanical non-linearities have been considered in soft tissue deformation simulations [18]–[24]. Among many available non-linear models, neo-Hookean hyperelastic models [25] are suitable for rubbery-like material and can be accurate models for soft tissue. Nienhuys and van der Stappen [20] simulated insertion of a rigid needle into a totally compressible (zero Poisson's ratio) neo-Hookean material model. Although their method can be extended to 3D, they performed the simulation in 2D. In [24] effects of the boundary conditions and non-linearities on targeting accuracy were shown by simulation of needle insertion into a compressible neo-Hookean material model under plane stress assumption. By contrast, in this paper the neo-Hookean material model is used in a 3D needle insertion simulation.

III. SIMULATION METHOD

The optimization method in this paper is an iterative method which uses the simulation results in each iteration to improve the insertion parameters. To simulate the needle insertion procedure a simplified 3D mesh of the prostate - a cube of material simulating the prostate tissue and surrounding tissue (see Fig. 2) - is used in an FEM simulation.

The simulation is performed in a *quasi-static* mode in which the tissue is assumed to be in its equilibrium at each time sample. The *stick-slip* model introduced in [4] is used to simulate the friction and cutting forces applied by the needle to the tissue. In this method, a node is *stuck* to the needle as long as its reaction force is less than a pre-defined threshold. Three displacement boundary conditions are applied to the stuck node. If the reaction force is greater than the threshold

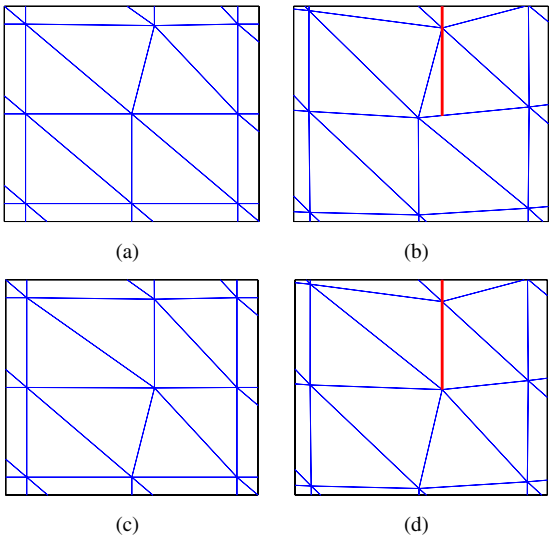

Fig. 3. Mesh adaptation algorithm. (a) and (b): The undeformed and deformed configurations, respectively, before mesh adaptation. The needle tip is close to a new element boundary. (c): The closest node to the needle tip is moved to the proper position in the undeformed configuration, without any external force. (d): The node is located at the needle tip in the deformed configuration.

the node state changes to *slip* mode. In this mode the node can freely slide along the needle. A force boundary condition is applied to the slipping node in the needle axial direction. Two displacement boundary conditions are applied to the same node to keep it on the needle.

During insertion the needle may enter an element from any point on the surface of the element, while the slip-stick force model applies the boundary conditions only to the element nodes. A mesh adaptation algorithm is used to solve this problem [5]. When the needle tip comes close to an element edge, the closest node to the needle tip is relocated onto the needle tip and the FEM model is updated to account for this change. Fig. 3(b) shows the deformed configuration of the mesh when the needle tip is close to a new element boundary. The corresponding undeformed (reference) mesh is shown in Fig. 3(a). Figs. 3(c) and 3(d) show the undeformed and deformed configurations, respectively, after mesh adaptation. In Fig. 3(d) the closest node to the needle tip is relocated on the needle tip. Since this node is relocated in the reference mesh, as shown in Figs. 3(a) and 3(c), no external force is applied to the node.

A. Non-linear Material Model

A neo-Hookean material model is used to accommodate both geometric and mechanical non-linearities. This model can simulate the prostate rotation and avoid element inversion in cases with high strain that can occur during needle insertion. The stored energy density for a neo-Hookean material that includes the compressibility effect is expressed as [25]:

$$W(I,J) = \frac{1}{2}\mu\left(I - 3 - 2\ln J\right) + \frac{1}{2}\lambda\left(J-1\right)^2, \quad (1)$$

where I is the first invariant of the deformation tensor and J is the determinant of the deformation gradient tensor. λ and μ are Lamé parameters. The Green strain, the second Piola-Kirchhoff stress and the material moduli tensors with respect to the reference configuration can be written as:

$$\begin{aligned} \epsilon_{ij} &= \frac{1}{2}(C_{ij} - \delta_{ij}), & (2)\\ \sigma_{ij} &= \mu\left(\delta_{ij} - C^{-1}_{ij}\right) + \lambda J\left(J-1\right)C^{-1}_{ij}, & (3)\\ D_{ijkl} &= \lambda J\left(2J-1\right)C^{-1}_{ij}C^{-1}_{kl} \\ &+ 2\left[\mu - \lambda J\left(J-1\right)\right]\mathcal{C}^{-1}_{ijkl}, & (4) \end{aligned}$$

where $i,j,k,l \in \{1,2,3\}$, δ_{ij} is Kronecker delta, C is the right Cauchy-Green deformation tensor, C^{-1}_{ij} is the pivot (i,j) of C^{-1} and:

$$\mathcal{C}^{-1}_{ijkl} = \frac{1}{2}\left[C^{-1}_{ik}C^{-1}_{jl} + C^{-1}_{il}C^{-1}_{jk}\right]. \quad (5)$$

Discretization and approximation of these equations over several finite elements lead to a set of non-linear algebraic equations of the form:

$$\Phi(\underline{u}) - \underline{f} = 0, \quad (6)$$

where $\underline{u}$ and $\underline{f}$ are vectors of nodal displacements and external forces, respectively. The Newton-Raphson method is used to iteratively solve the non-linear equations of deformation [25]. Therefore, the following equation should be solved for $\delta\underline{u}$ at each iteration:

$$\mathbf{K_T}(\underline{u}^t)\ \delta\underline{u}^{t+1} = -(\Phi(\underline{u}^t) - \underline{f}) = -\underline{e}^t, \quad (7)$$

where $\mathbf{K_T}$ is the tangent stiffness matrix constructible from (2)-(5), $\underline{u}^t$ is the vector of nodal displacements in iteration t, $\underline{e}^t$ is the vector of error and:

$$\underline{u}^{t+1} = \underline{u}^t + \delta\underline{u}^{t+1}. \quad (8)$$

IV. OPTIMIZATION ALGORITHM

The non-linear FEM simulator described above works as a function in the optimization program. The needle insertion point p_s, the insertion depth d and the needle heading v are the inputs of this function. The outputs are the displaced target positions u_i:

$$u_i = f_i(p_s, v, d) \qquad i \in \{1,2,\cdots,N\}, \quad (9)$$

where N is the number of targets. It is assumed that u_N is the displaced position of the distal target. Tissue elastic parameters, target initial positions and stick-slip model parameters are assumed to be known constants in this function.

The optimization goal is to minimize the distance between the displaced targets and a rigid needle in the deformed configuration by optimizing the needle insertion point, heading and depth. Assume a global coordinate system $Oxyz$ and a needle-attached coordinate system $Ox_Ny_Nz_N$ as shown in Fig. 2. Since the needle is axially symmetric, only the pitch and yaw angles are necessary to determine the relation between the two coordinate systems. In addition to the pitch and yaw angles, the needle insertion point in the $x-z$

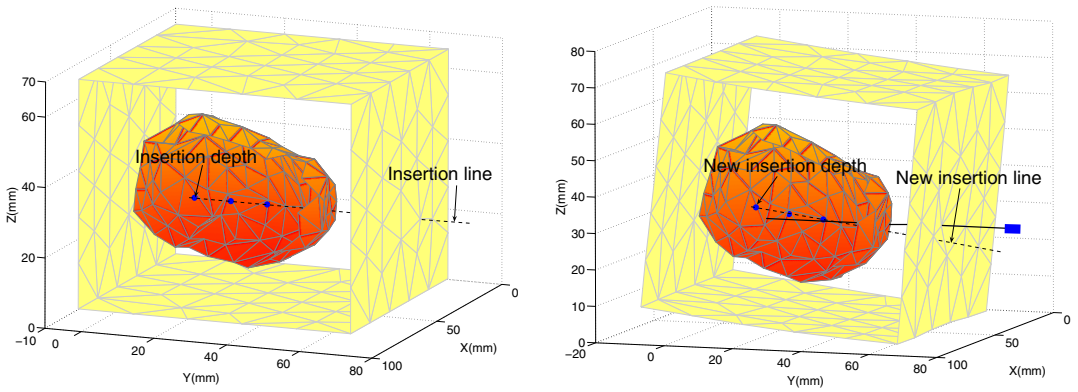

(a) The undeformed configuration

(b) After the first iteration

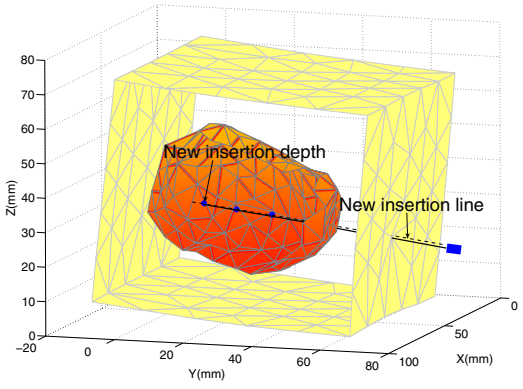

(c) After the second iteration

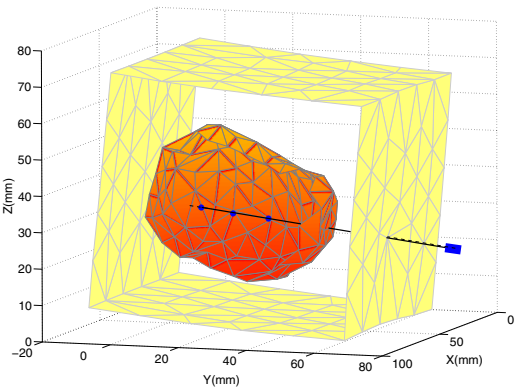

(d) After the third iteration

Fig. 4. Simulation iterations for three targets. (b), (c) and (d) show the position of the targets in the deformed tissue after insertion of the needle with the insertion parameters calculated in (a), (b) and (c), respectively. 3D fitted line is shown as a dotted line. The front surface of the prostate mesh is removed to show the position of the targets and the needle inside.

plane and the insertion depth are the other parameters to be optimized.

Consider the deformed configuration of the tissue after the insertion of the needle from a point on the tissue surface along a specified direction (see i.e. Fig. 4(b)). Due to deformations caused by needle forces, the targets are displaced. In this situation, the next candidate for needle insertion heading is the 3D line fitted to the displaced targets. The following steps are used in an iterative algorithm to optimize the insertion parameters:

1) Align the needle with the 3D line passing through the targets in the undeformed configuration. This line can be defined by a point p and a vector v. The insertion point is the intersection of this line and the front surface of the tissue. The insertion depth is defined as the distance between the distal target and the front surface of the tissue (see Fig. 4(a)).
2) Insert the needle from the insertion point along the computed insertion line to the desired depth. Find the displaced target positions u_i as in (9) using the FEM simulator.
3) Fit a 3D line to the displaced targets in the deformed tissue (see Figs. 4(b)-4(d)). The new line parameters can be computed by solving the following problem.

$$(p^{k+1}, v^{k+1}) = \arg\min_{p,v} \sum_{i=1}^{N} \min_{\alpha} \|p + \alpha v - u_i^k\|^2, \tag{10}$$

where k is the iteration number. It can be shown that:

$$p^{k+1} = \frac{1}{N} \sum_{i=1}^{N} u_i^k \tag{11}$$

$$v^{k+1} = \arg\max_{v} \frac{\|\mathbf{A}v\|}{\|v\|}, \tag{12}$$

where

$$\mathbf{A} = \left[u_1^k - p^{k+1} \;\; u_2^k - p^{k+1} \cdots \;\; u_N^k - p^{k+1}\right]^T. \tag{13}$$

Therefore v^{k+1} is the right singular vector corresponding to the largest singular value of $\mathbf{A}$.
4) The new insertion point p_s^{k+1}, is the intersection of the insertion line and the front surface of the tissue.
5) The distance between the insertion point and the closest point on the insertion line to the distal target in

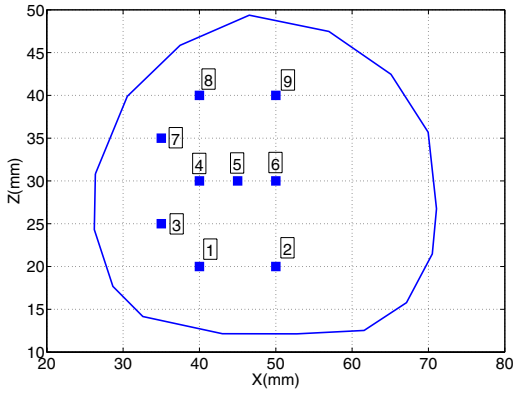

Fig. 5. The $x-z$ position of the target sets in a cross section of the prostate at $y = 25\text{mm}$.

the deformed configuration is the new insertion depth. This can be written as:

$$d^{k+1} = \arg\min_{\alpha} \|p_{\text{s}}^{k+1} + \alpha v - u_N^k\|^2 \qquad (14)$$

6) If the convergence criterion is met, then terminate the algorithm. Otherwise go to step 2.

The convergence criterion could be the satisfaction of a bound on the sum of distances from the displaced targets to the needle. Targets in brachytherapy are originally on a straight line in the undeformed tissue. However, after deformation it is usually impossible for the displaced targets to be on a straight line. Therefore, the above mentioned convergence criterion does not usually converge to zero. Alternatively, convergence of the optimization parameters to a value can be used as the convergence criterion. In this method if the Euclidean norm of the difference between two consecutive vectors of parameters is less than a threshold the algorithm is terminated (see Fig. 4(d)).

V. SIMULATION RESULTS

The optimization algorithm was performed for nine sets of targets, each of which consisted of three targets located inside the prostate mesh as shown in Fig. 4(a). The targets in each set were localized on a straight line parallel to the y axis in the undeformed configuration at $y = 15$, $y = 25$ and $y = 35$ mm. Fig. 5 shows the $x-z$ coordinates of the nine target sets in a cross section of the prostate at $y = 25\text{mm}$. The tissue elastic parameters were typical of soft tissue and are given, together with other simulation parameters, in Table I.

The optimization algorithm was performed for each of the target sets. The optimization iterations were continued until the change in the vector of parameters was less than 1%. The sums of distances from the three targets to the needle at the first and the last iterations are reported in Table II for each set. It can be seen that in all the cases the algorithm converged in 3 to 7 iterations to sub-millimeter errors. In the final iteration, the targets lie very close to the needle and the errors are less than the brachytherapy needle diameter.

As an example, Fig. 4(a) shows the position of the targets inside the tissue in the undeformed configuration for the 5^{th} set. Figs. 4(b)-4(d) show the configuration of the deformed tissue after each iteration. The optimization algorithm converged in 3 iterations. It can be seen in Fig.4(d) that the needle path is very close to the computed insertion line for the next iteration. The target positions and the optimized parameters for this case are shown in Table III.

TABLE I
SIMULATION PARAMETERS

(λ, ν) for the prostate tissue	(9.8×10^5, 2.01×10^4)
(λ, ν) for the surrounding tissue	(3.3×10^5, 6.7×10^3)
Number of Nodes	570
Number of Elements	2801
Element Type	Tetrahedron
Simulation type	Non-linear, quasi-static
Material Type	Compressible neo-Hookean

TABLE II
SIMULATION RESULTS SHOWING THE ERROR BEFORE AND AFTER OPTIMIZATION

Set	Number of Iterations	1^{st} Iteration Error (mm)	Last Iteration Error (mm)
1	3	15.5	0.6
2	7	11.5	0.9
3	6	13.0	0.4
4	3	7.4	0.7
5	3	7.5	0.8
6	6	4.9	0.7
7	3	7.8	0.3
8	4	4.4	0.7
9	3	2.4	0.4

For each iteration of the optimization, a needle insertion process into a non-linear material model was simulated. At each time step a set of non-linear algebraic equations had to be solved due to the non-linearity of the material model. These equations were solved iteratively using the Newton-Raphson method. The tangent stiffness matrix in (7) was of dimension 1710×1710. Therefore, the simulation part was very time consuming. The mean time per simulation was 70 minutes using Matlab®. When higher speeds are required linear tissue models can be used. Simulation acceleration methods for linear models can be used to increase the simulation speed dramatically as in [26] in which the simulation time was decreased to 50 seconds. Although quasi-Newton methods are available to increase the computation speed for non-linear models, linear models are considerably faster. With optimization of the computer code in C++ faster solutions are possible.

The Newton-Raphson method employed to solve the non-linear FEM equations converged to the desired error, described in (7), in less than 10 iterations in all of the performed simulations, while convergence was achieved in 5 iterations most of the time.

VI. CONCLUSIONS AND FUTURE WORKS

A. Conclusion

The needle insertion point, heading and depth were optimized using an optimization method for a prostate brachytherapy simulator. To simulate the prostate rotation

TABLE III

SIMULATION RESULTS FOR THE 5^{th} SET

1^{st} target location (mm)	$(45, 15, 30)$
2^{nd} target location (mm)	$(45, 25, 30)$
3^{rd} target location (mm)	$(45, 35, 30)$
Optimized needle insertion point (mm)	$(43.1, 70, 25.9)$
Optimized insertion depth (mm)	59.0
Optimized needle orientation (yaw, pitch)	$(7.84^{\text{o}}, -2.97^{\text{o}})$

a neo-Hookean non-linear material model was used to consider geometric and mechanical non-linearities as well as compressibility effects. The optimization algorithm showed convergence in a few iterations and decreased the seed misplacement errors effectively. Since non-linear models were applied in the simulation phase, the program was computationally expensive. Linear simulation methods can be used to increase the optimization speed. The optimization method can be used with any model for tissue deformation simulation, since the assumptions on the simulation phase do not put any restrictions on the optimization phase.

B. Future Work

In the future, validation studies will be carried out using a needle guidance robot to orient and insert the needle into tissue phantoms. A tissue phantom is needed to simulate the prostate and surrounding tissue. This tissue phantom should have accurate boundary conditions and be able to mimic the rotation of the prostate around the pubic bone. Needle flexibility will be added to the planning system. In this case the needle insertion point and orientation for a rigid needle will be used as a starting point for the flexible needle. Needle base manipulation methods introduced in [11] or [12] could be used to steer the needle for smaller targeting errors inside the prostate.

REFERENCES

[1] V. Lagerburg, M. A. Moerland, J. J. Lagendijk, and J. J. Battermann, "Measurement of prostate rotation during insertion of needles for brachytherapy," *Radiotherapy and Oncology*, vol. 77, pp. 318–323, 2005.

[2] R. Teschereau, J. Pouliot, J. Roy, and D. Tremblay, "Seed misplacement and stabilizing needles in transperineal permanent prostate implants," *Radiotherapy and Oncology*, vol. 55, pp. 59–63, 2000.

[3] Z. Wei, G. Wan, L. Gardi, G. Mills, D. Downey, and A. Fenster, "Robot-assisted 3D-TRUS guided prostate brachytherapy: System integration and validation," *Medical Physics*, vol. 31, pp. 539–548, 2004.

[4] S. P. DiMaio and S. E. Salcudean, "Needle insertion modeling and simulation," *IEEE Transaction on Robotics and Automation: Special Issue on Medical Robotics*, vol. 19, pp. 864 – 875, 2003.

[5] O. Goksel, S. E. Salcudean, S. P. DiMaio, R. Rohling, and J. Morris, "3D needle-tissue interaction simulation for prostate brachytherapy," in *Proc. Medical Image Computing and Computer Assisted Intervention (MICCAI)*, 2005, pp. 827–834.

[6] R. Alterovitz, J. Pouliot, R. Taschereau, I. C. Hsu, and K. Goldberg, "Simulating needle insertion and radioactive seed implantation for prostate brachytherapy," in *Medicine Meets Virtual Reality 11*, January 2003, pp. 19–25.

[7] ——, "Sensorless planning for medical needle insertion procedures," in *Proc. IEEE/RSJ International Conference on Intelligent Robots and Systems*, vol. 3, 2003, pp. 3337–3343.

[8] R. J. Webster III, N. J. Cowan, G. S. Chirikjian, and A. M. Okamura, "Nonholonomic modeling of needle steering," in *Proc. 9th International Symposium on Experimental Robotics*, June 2004, pp. 3337–3343.

[9] R. Alterovitz, K. Goldberg, and A. Okamura, "Planning for steerable bevel-tip needle insertion through 2D soft tissue with obstacles," in *Proc. IEEE International Conference on Robotics and Automation*, 2005, pp. 1640 – 1645.

[10] R. Alterovitz, A. Lim, K. Goldberg, G. S. Chirikjian, and A. M. Okamura, "Steering flexible needles under markov motion uncertainity," in *IEEE/RSJ International Conference on Intelligent Robots and Systems*, 2005.

[11] S. P. DiMaio and S. E. Salcudean, "Needle steering and motion planning in soft tissue," *IEEE Transaction on Biomedical Engineering*, vol. 52, pp. 965 – 974, 2005.

[12] D. Glozman and M. Shoham, "Flexible needle steering and optimal trajectory planning for percutaneous therapies," in *Proc. Medical Image Computing and Computer Assisted Intervention*. Springer-Verlag, 2004, pp. 137–144.

[13] E. Dehghan, O. Goksel, and S. E. salcudean, "A comparison of needle bending models," in *Proc. Medical Image Computing and Computer Assisted Intervention (MICCAI)*, 2006, pp. 305–312.

[14] N. Abolhassani, R. Patel, and M. Moallem, "Trajectory generation for robotic needle insertion in soft tissue," in *Proc. Int. Conf. Engineering in Medicine and Biology Society*, 2004, pp. 2730–2733.

[15] M. Heverly, P. Dupont, and J. Triedman, "Trajectory optimization for dynamic needle insertion," in *Proc. of IEEE International Conference on Robotics and Automation*, 2005, pp. 1646 – 1651.

[16] A. Okamura, C. Simone, and M. O'Leary, "Force modeling for needle insertion into soft tissue," *IEEE Transactions on Biomedical Engineering*, vol. 51, pp. 1707 – 1716, 2004.

[17] H. Kataoka, T. Washio, K. Chinzei, K. Mizuhara, C. Simone, and A. Okamura, "Measurement of tip and friction force acting on a needle during penetration," in *Proc. Medical Image Computing and Computer Assisted Intervention (MICCAI)*, T. Dohi and R. Kikinis, Eds., 2002, vol. 2488, pp. 216–223.

[18] G. Picinbono, H. Delingette, and N. Ayache, "Nonlinear and anisotropic elastic soft tissue models for medical simulation," in *Proc. IEEE International Conference on Robotics and Automation*, vol. 2, 2001, pp. 1370–1375.

[19] Y. Zhuang and J. Canny, "Haptic interaction with global deformations," in *Proc. IEEE Int. Conf. Robotics and Automation*, 2000, pp. 2428 – 2433.

[20] H. W. Nienhuys and A. F. van der Stappen, "A computational technique for interactive needle insertions in 3D nonlinear material," in *Proc. IEEE International Conference on Robotics and Automation*, vol. 2, 2004, pp. 2061 – 2067.

[21] X. Wu, M. S. Downes, T. Goktekin, and F. Tendick, "Adaptive nonlinear finite elements for deformable body simulation usind dynamic progressive meshes," *IEEE Transaction on Visualization and Computer Graphics*, vol. 5, no. 1, pp. 62–73, 1999.

[22] F. M. Hendriks, D. Brokken, J. T. van Eemeren, C. W. Oomens, F. P. Baaijens, and J. B. Horsten, "A numerical-experimental method to characterize the non-linear mechanical behavior of human skin," *Skin Research Technology*, vol. 9, no. 3, pp. 274–283, 2003.

[23] M. Chabanas, Y. Payan, C. Marecaux, P. Swider, and F. Boutault, "Comparison of linear and non-linear soft tissue models with post-operative ct scan in maxillofacial surgery," *Lecture Notes in Computer Science*, vol. 3078, pp. 19–27, 2004.

[24] E. Dehghan and S. E. Salcudean, "Comparison of linear and non-linear models in 2D needle insertion simulation," in *Proc. Workshop on Computational Biomechanics for Medicine (In conjunction with MICCAI)*, 2006, pp. 117–124.

[25] O. C. Zienkiewicz and R. L. Taylor, *The Finite Element Method: Solid Mechanics*, 5th ed. Butterworht-Heinemann, 2000, vol. 2.

[26] E. Dehghan and S. E. Salcudean, "Needle insertion point and heading optimization with application to brachytherapy," in *Proc. Workshop on Medical Robotics (In conjunction with MICCAI)*, 2006, pp. 47–53.